Analyst

Dynamic Article Links

Cite this: *Analyst*, 2012, **137**, 1649

www.rsc.org/analyst

PAPER

Two-peak approximation in kinetic capillary electrophoresis†

Leonid T. Cherney and Sergey N. Krylov*

Received 6th December 2011, Accepted 5th February 2012
DOI: 10.1039/c2an16218k

Kinetic capillary electrophoresis (KCE) constitutes a toolset of homogeneous kinetic affinity methods for measuring rate constants of formation (k_+) and dissociation (k_-) of non-covalent biomolecular complexes, C, formed from two binding partners, A and B. A parameter-based approach of extracting k_+ and k_- from KCE electropherograms relies on a small number of experimental parameters found from the electropherograms and used in explicit expressions for k_+ and k_- derived from approximate solutions to mass transfer equations. Deriving the explicit expressions for k_+ and k_- is challenging but it is justified as the parameter-based approach is the simplest way of finding k_+ and k_- from KCE electropherograms. Here, we introduce a unique approximate analytical solution of mass transfer equations in KCE termed a "two-peak approximation" and a corresponding parameter-based method for finding k_+ and k_-. The two-peak approximation is applicable to any KCE method in which: (i) A* binds B to form C* (the asterisk denotes a detectable label on A), (ii) two peaks can be identified in a KCE electropherogram and (iii) the concentration of B remains constant. The last condition holds if B is present in access to A* and C* throughout the capillary. In the two-peak approximation, the labeling of A serves only for detection of A and C and, therefore, is not required if A (and thus C) can be observed with a label-free detection technique. We studied the proposed two-peak approximation, in particular, its accuracy, by using the simulated propagation patterns built with the earlier-developed exact solution of the mass-transfer equations for A* and C*. Our results prove that the obtained approximate solution of mass transfer equations is correct. They also show that the two-peak approximation facilitates finding k_+ and k_- with a relative error of less than 10% if two peaks can be identified on a KCE electropherogram. Importantly, the condition of constant concentration of B is always satisfied in macroscopic approach to studying kinetics at equilibrium (MASKE) whether or not B is in excess to A* and C*, and, thus, the two-peak approximation is applicable to MASKE. It completes a toolset of fitting-free methods for processing MASKE data and makes MASKE a simple practical method for finding k_+ and k_- of "fast", "slow", and "intermediate-rate" non-covalent interactions.

Introduction

The association of biological molecules into non-covalent complexes is an important phenomenon. A vast number of studies showed that the formation of such complexes plays a key role in regulation of cellular processes, such as enzyme activation, transport across membranes, cell signaling, DNA replication, gene expression, *etc*.[1–5] On the other hand, undesirable protein aggregation can lead to the formation of pathological structures that cause, for example, prion and amyloid diseases.[6,7]

In order to use non-covalent macromolecular interactions in a variety of biomedical applications, a better understanding of such interactions is required. This requires, in particular, studies of kinetics and thermodynamics of non-covalent complex formation. To date, several methods have been developed to measure kinetic and thermodynamic constants of complex formation and dissociation.[8–37] One of such methods is surface plasmon resonance (SPR), in which one reactant, A, is immobilized on a solid sensor surface, whereas the other reactant, B, is free in solution contacting the surface with reactant A.[8] In SPR, the complex C is formed on the surface, and the kinetics of complex formation and dissociation is monitored under the condition of perturbed equilibrium caused by a change in the concentration of B on the sensor. SPR belongs to a group of heterogeneous methods. They all suffer from non-specific binding of reactant B to the surface. In addition, the immobilization of A on the surface can change its affinity to B. Homogeneous methods include, for example, affinity capillary electrophoresis (ACE) metods[9–12] and kinetic capillary electrophoresis (KCE) methods[13–20] that manipulate the concentrations

Department of Chemistry and Centre for Research on Biomolecular Interactions, York University, Toronto, Ontario M3J 1P3, Canada. E-mail: skrylov@yorku.ca; Fax: +416-736-5936; Tel: +416-736-2100 x 22345

† Electronic supplementary information (ESI) available. See DOI: 10.1039/c2an16218k

of A, B, and C in solution *via* their differential electrophoretic mobilities. KCE methods use perturbed-equilibrium conditions and can work in a wide range of rate constants. ACE and KCE methods were successfully applied to kinetic and thermodynamic studies of macromolecular complexes[21–29] and to the selection of DNA aptamers.[30–34] KCE methods often require a non-uniquely defined iterative procedure of fitting the calculated reactant concentrations into the experimental data. Microscopic methods of measuring rate constants k_+ and k_- are usually more complicated since these methods require monitoring concentrations in microscopic volumes. They include for example nanopore amperometry, fluorescence correlation spectroscopy, and fluorescence resonance energy transfer.[35–37] The microscopic methods deal with small reactor volumes and a small number of molecules in the reactor. As a result, many convenient and informative detection methods (such as mass spectrometry) cannot be used.

Macroscopic approach to studying kinetics at equilibrium (MASKE) allows the determination of the rate constants at chemical equilibrium.[38] MASKE utilizes two mixtures, non-labeled and labeled, in two following reactions, respectively:

$$\mathrm{A} + \mathrm{B} \underset{k_-}{\overset{k_+}{\rightleftharpoons}} \mathrm{C} \qquad (1)$$

$$\mathrm{A}^* + \mathrm{B} \underset{k_-}{\overset{k_+}{\rightleftharpoons}} \mathrm{C}^* \qquad (2)$$

Components A and B are binding partners and C is their non-covalent complex. The asterisk denotes a detectable label on A that does not significantly affect the rate constants k_+ and k_-, which is typically true if A is a big molecule such as an oligonucleotide or protein. Also, the label is assumed not to significantly change the physical properties of A and C, such as their electrophoretic mobilities. MASKE can be implemented by using a capillary as a reactor and electrophoresis as the driving force of separating A from C. The reactor is filled with the non-labeled mixture along all its length except for a small portion where a plug of the labeled mixture is placed (Fig. 1a). The MASKE setup requires the maintenance of a chemical equilibrium between A + A*, B, and C + C*:

$$(\mathrm{A} + \mathrm{A}^*) + \mathrm{B} \underset{k_-}{\overset{k_+}{\rightleftharpoons}} (\mathrm{C} + \mathrm{C}^*), \quad K_\mathrm{d} = k_-/k_+ \qquad (3)$$

which itself requires a more experimental setup than in other KCE methods. As a result of such equilibrium, the concentrations of A + A*, B, and C + C* do not change with time or spatial coordinate, which, in turn, leads to the existence of an exact solution of the mass transfer equations for A* and C* in MASKE.[38] Though this solution is fairly complicated, it allows one to numerically build simulated label-propagation patterns. The latter can be fitted into the experimental patterns through non-linear regression by varying k_+ and k_- and until the best fit is found.

The pattern-based approach to finding rate constants requires the knowledge of the label distribution in the initial zone of the labeled mixture. Otherwise, this distribution must be included into a set of parameters that have to be fitted. The use of too many unknown parameters in the fitting procedure could result in lower accuracy of found k_+ and k_-. Indeed, sometimes it is not clear if the best fit is achieved due to a correct determination of k_+ and k_- or due to an incorrect choice of the unknown initial label distribution. Besides, the fitting procedure requires substantial computation time (several hours) even with modern computers. The pattern-based approach is also used in other KCE methods of rate constant determination.[13–17] An alternative parameter-based approach relies on obtaining a small number of characteristic parameters from experimental label-propagation patterns.[38–40] These parameters can be utilized to calculate k_+ and k_-, using relatively simple approximate solutions to differential equations for mass transfer of the labeled components. Finding such approximate solutions is challenging and usually each solution only serves for a limited range of k_+ and k_-. However, if multiple solutions are found to cover a whole range of physically attainable k_+ and k_-, such solutions serve as the simplest way of extracting kinetic data from KCE electropherograms. The simplicity of the parameter-based approach of finding k_+ and k_- in KCE is the major motivation of our current effort towards deriving approximate solution of mass-transfer equations in KCE.

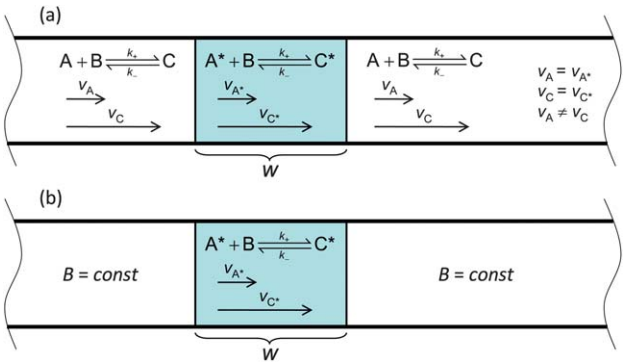

Fig. 1 Illustration of two types of initial conditions with a single plug of the labeled mixture (shaded) of A* and C* being a common feature: a) a more constrained MASKE setup with the labeled-mixture plug surrounded by the non-labeled mixture of A and C and b) a general "two-peak approximation" setup in which the presence of A and C outside of the labeled-mixture plug is not necessary if B is present in access to A* and C* and, therefore, its concentration, B, remains constant.

In the present work, we report an approximate analytical solution of mass transfer equations in KCE and a corresponding simple parameter-based method for finding k_+ and k_-.

Results and discussion

Two-peak approximation approach

We study a non-equilibrium reaction (2) in a general case when two peaks can be identified in KCE electropherograms of the mixture of A* and C* (Fig. 2a and 2b) provided that the concentration of B remains constant in the reaction (2). This condition can be satisfied in various experimental setups. For example, the constancy of the concentration of B can be readily achieved if the total amount of B (in free and complexed forms) is in access of the total amount of A* (in free and complexed forms) or if B is equilibrated with its dimer B_2 that is present in excess to B. In the latter case the concentration B itself can be of the same order of magnitude as the concentrations of A* and C*. In such setups, the presence of A and C outside the plug are not required

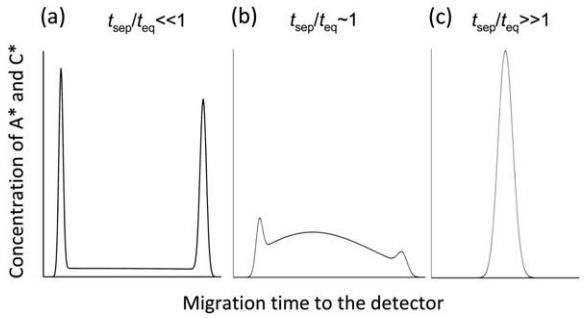

Fig. 2 Three types of temporal propagation patterns of the mixture of A* and C* depending on ratios between the characteristic separation and equilibration times, t_{sep}/t_{eq}: (a) two narrow peaks with a low "bridge" between them at slow equilibration, (b) two peaks with a high "bridge" at moderate-rate equilibration, and (c) a single peak at fast equilibration. Parameters t_{sep} and t_{eq} are defined by eqn (5).

at all (Fig. 1b) and the labeling of A and C inside the plug serves only for their sensitive detection and identification of the two peaks. Therefore, the labeling is not required if the peaks can be observed with a label-free detection technique. Finally, the constancy of concentration of B is always achieved in MASKE. However, in MASKE, the labeling of A and C in the "labeled mixture" is absolutely required. Thus, the general setup with constant B considered in this work has a wider area of applications than the MASKE setup does. In particular, the developed approximate solution of mass transfer equations is valid for non-equilibrium reaction (2) and, therefore, can be used in non-equilibrium KCE methods. The proposed way of finding k_+ and k_- utilizes only the parameters associated with the two peaks. We coin the term of "a two-peak approximation in KCE" for the developed analytical solution of mass transfer equation and a corresponding method for finding k_+ and k_-.

Conditions required for the applicability of the proposed two-peak approximation method can be tested by different means. Regarding the constancy of B, it would be usually enough to verify that B was taken in excess to A during the preparation of both the plug and the buffer outside the plug. The constancy of B can be tested more accurately by measuring the background signal in separate experiments with B also labeled. The presence of two distinguishable peaks is often evident from electropherograms. The assignment of these peaks to components A* and C* can be verified by other KCE methods, in particular, by non-equilibrium capillary electrophoresis of equilibrium mixture (NECEEM).[13–16] These methods also allow one to exclude a possible formation of larger complexes in addition to the bimolecular ones. Prior knowledge about reactions (1) and (2), such as identities and some properties of the reactants (and the label if there is one), are also required. In particular, it should be known that reactants are not prone to the formation of multi-molecular complexes since the two-peak approximation is developed specifically for biomolecular reactions (1) and (2).

To develop the two-peak approximation, we transformed partial differential equations for the local concentrations of A* and C* into ordinary differential equations for the total amounts of A* and C* in the peaks. The obtained ordinary differential equations were solved; as a result, approximate algebraic relations between k_+ and k_- and a number of parameters characterizing the temporal propagation patterns of mixture of A* and C* were found. These parameters include: (i) the total amounts of mixture of A* and C* in the peaks flanking the bridge (see Fig. 2a and 2b); and (ii) migration times of the peaks to a detector. To obtain the required parameters, two experiments would be sufficient. They must be performed under similar conditions, with the only difference being the distance from the initial position of the plug to the detector. We tested the proposed approach using numerically simulated propagation patterns of mixture of A* and C*. These patterns were obtained with the exact solution of the mass transfer equations for A* and C* in the case B remaining constant that was developed elsewhere.[38] The original values of k_+ and k_- are obviously known in such simulated experiments, which makes them the best testing tool. The calculated patterns also allowed us to study the accuracy of the determination of k_+ and k_- by the two-peak approximation. The results show that the values of determined k_+ and k_- are very close to the ones used in the simulation. The developed approach can be applicable to highly-selective interactions of biomolecules, which typically interact with lower k_+ and k_-. Such reactions are more likely characterized by equilibration times that are comparable to (or greater than) the separation times in capillary electrophoresis and, therefore, the two peaks can be identified in the electropherograms (Fig. 2a and 2b). The two-peak approximation can be also applied to the MASKE method as B always remains constant in MASKE. When added to the previously developed parameter-based method for fast equilibration,[38] the two-peak approximation completes a toolset of fitting-free approaches for MASKE. This also makes MASKE a simple practical method for finding the widest range of k_+ and k_-.

Approximate solution of mass transfer equations

We consider the following setup for the two-peak approximation in KCE (see Fig. 1b). A long and narrow capillary is coaxial with the x coordinate. The velocities and initial concentrations of components do not change significantly across the capillary. The longitudinal Peclet number is very large. Such a reactor can usually be considered as a one-dimensional infinite reactor, in which longitudinal diffusion is negligible. A reversible binary reaction (2) of the components A* and B results in the affinity complex C* = A*B. Generally speaking, chemical reaction (2) is in its non-equilibrium state and is characterized by rate constants of the forward and reverse processes, k_+ and k_-, respectively. Mass transfer of A* and C* is described by the following equations:

$$\begin{aligned}(\partial_t + v_A\partial_x)A^* &= -k_+A^*B + k_-C^*\\ (\partial_t + v_C\partial_x)C^* &= k_+A^*B - k_-C^*\end{aligned} \quad (4)$$

where ∂_x and ∂_t are partial derivations by the spatial coordinate and time, respectively; A^* and C^* are linear concentrations of A* and C*, respectively (*i.e.* amounts of A* and C* per unit length of the reactor); B is a volume concentration of B that remains constant throughout the capillary ($B = const$); and v_A and v_C are the velocities of A* and C*. Hereafter the asterisk can be omitted if the labeling of A and C in the plug is not required for the detection of peaks.

We assume that components A* and C* are introduced in the initial zone of spatial width W (along the capillary) at $t = 0$. After that (at $t > 0$) distributions of A* and C* are defined by two simultaneous processes that are described by eqn (4). The first process is the movement of A* and C* with different velocities (we assume for definitiveness that $v_C > v_A > 0$) that results in their separation. The second process is the forward and reverse reactions (2) between A*, B, and C* that lead to equilibration between A* and C*. The characteristic times of separation and equilibration, t_{sep} and t_{eq}, respectively, are given by:[39]

$$t_{sep} = \frac{W}{|v_C - v_A|}, \quad t_{eq} = \frac{1}{k_+B + k_-} \tag{5}$$

Definition (5) of t_{sep} is based on the full width W of the initial zone, which corresponds to an upper estimate for t_{sep}. If the concentration profile in the initial zone is modeled by the Gaussian distribution, then W is defined as the distance between points where the total concentration of A* and C* is equal to 1% of its maximum value.

If $t_{sep} \ll t_{eq}$ or $t_{sep} \sim t_{eq}$, two peaks of the mixture of A* and C* can be observed for some time after introducing this mixture as the initial zone of width W and starting the separation (Fig. 2). These peaks move with velocities v_A and v_C. We will denote them as zones (or peaks) A* and C*, respectively, since they mainly contain intact components A* and C*. The existence of such zones allows the following approximate equations to be derived from basic eqn (4) (see the **Supplementary Information**†):

$$\frac{dA_a^*}{dt} = -k_+BA_a^* + k_-C_a^*, \quad \frac{dC_a^*}{dt} = k_+BA_a^* - \left(k_- + \frac{3}{t_{sep}}\right)C_a^*, \tag{6}$$

$$\frac{dA_c^*}{dt} = -\left(k_+B + \frac{3}{t_{sep}}\right)A_c^* + k_-C_c^*, \quad \frac{dC_c^*}{dt} = k_+BA_c^* - k_-C_c^* \tag{7}$$

Here, d/dt is the ordinary derivation by time, A^*_a and C^*_a are the total amounts of A* and C* in zone A*. Similarly, A_c^* and C_c^* are the total amounts of A* and C* in zone C*. Hereafter, lowercase subscripts a and c are used to denote characteristics of zones A* and C*, respectively. In contrast, capital subscripts A and C indicate characteristics of components A* and C* themselves, such as velocities (v_A and v_C) or quantum yields (see relations (22) below).

Eqn (6) and (7) contain the ordinary derivation by time rather than the partial derivations by time and spatial coordinate, as the basic eqn (4) do. This fact tremendously simplifies the analysis of propagation of components A* and B*. Indeed, an exact solution to eqn (6) and (7) can be expressed in the following form (see derivations of (8)–(12) in the **Supplementary Information**†):

$$A_a^* = N_a\exp(-\lambda_a t), \quad C_a^* = \eta_a N_a\exp(-\lambda_a t) \tag{8}$$

$$A_c^* = \eta_c N_c\exp(-\lambda_c t), \quad C_c^* = N_c\exp(-\lambda_c t) \tag{9}$$

Here, N_a and N_c are non-negative constants that can be expressed in terms of the initial amounts of A* and C*. Coefficients λ_a, λ_c, η_a, and η_c depend on parameters Bk_+, k_-, and t_{sep} and are determined as follows:

$$\lambda_a = \Omega - \sqrt{\Omega^2 - \frac{3Bk_+}{t_{sep}}}, \quad \lambda_c = \Omega - \sqrt{\Omega^2 - \frac{3k_-}{t_{sep}}}, \tag{10}$$

$$\Omega \equiv \frac{1}{2}\left(Bk_+ + k_- + \frac{3}{t_{sep}}\right), \tag{11}$$

$$\eta_a = \frac{Bk_+ - \lambda_a}{k_-}, \quad \eta_c = \frac{k_- - \lambda_c}{Bk_+}. \tag{12}$$

Relations (10)–(12) result in η_a and η_c satisfying the following inequalities (see the **Supplementary Information**†):

$$\eta_a \geq 0, \quad \eta_c \geq 0 \tag{13}$$

Therefore, solutions (8) and (9) satisfy the requirement of non-negativity of A_a^*, C_a^*, A_c^*, and C_c^*. Eqn (8)–(12) constitute a core of two-peak approximation in KCE. They express reactant amounts in the peaks in a simple explicit form, which can facilitate simple data analysis in KCE and MASKE.

If the ratio t_{sep}/t_{eq} tends to zero, coefficients λ_a and λ_c are determined by the following simple relations (see the **Supplementary Information**†)

$$\lambda_a \approx Bk_+, \quad \lambda_c \approx k_- \quad (t_{sep} \ll t_{eq}). \tag{14}$$

In turn, relations (8), (9), and (12) guarantee that C_a^* and A_c^* approach zero if λ_a and λ_c approach Bk_+ and k_-, respectively. We can conclude that the structure of solutions (8) and (9) depends on the rate of equilibration in the following way. At moderate-rate equilibration (*i.e.* at $t_{sep}/t_{eq} \sim 1$), each of the zones A* and C* contains both A* and C* and each of the coefficients λ_a and λ_c depends on both rate constants. In contrast, at slow equilibration (*i.e.* at $t_{sep}/t_{eq} \ll 1$), each of zones A* and C* practically contains only a component after which this zone is named while the other (alien) component is depleted. Also, at slow equilibration, λ_a depends only on Bk_+ and λ_c depends only on k_- according to relations (14).

Rate constant determination by two-peak approximation

Solutions (8) and (9) yield the following expressions for the total amounts of the mixture of A* and C*, L_a and L_c, in zones A* and C*:

$$L_a \equiv A_a^* + C_a^* = (1 + \eta_a)N_a\exp(-\lambda_a t) \tag{15}$$

$$L_c \equiv A_c^* + C_c^* = (1 + \eta_c)N_c\exp(-\lambda_c t) \tag{16}$$

These relations allow the coefficients λ_a and λ_c to be determined if the amounts L_a and L_c are measured at some time $t > 0$. Importantly, this can be done even if the values of N_a and N_c are unknown. In this case, one should find the values of L_a at two different times, t_{a1} and t_{a2}, and also find the values of L_c at some other times, t_{c1} and t_{c2} (Fig. 3).

The substitution of these data, *i.e.* values of L_a and L_c and values of corresponding times, in (15) and (16) leads to a system of simple equations that yield the following expressions for the coefficients λ_a and λ_c (see the **Supplementary Information**†):

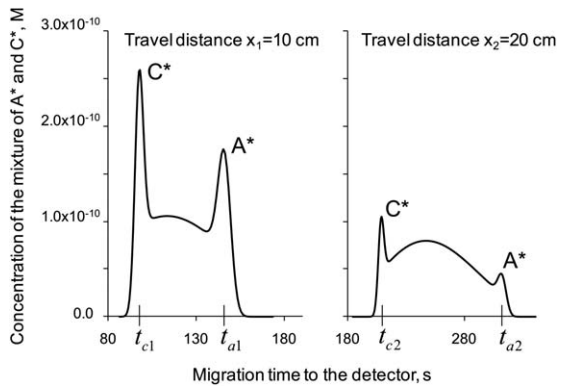

Fig. 3 Examples of simulated temporal propagation patterns of the mixture of A* and C*. Migration time is measured from the introduction of the initial plug. The peaks appear at different times for different travel distances x_1 and x_2 from the initial plug to the detector. At $v_C > v_A$, peak C* reaches the detector earlier than peak A*. As time increases, the peak heights and areas decrease, and the distance between the peaks grows.

$$\lambda_a = \frac{1}{t_{a2} - t_{a1}} \ln \frac{L_a(t_{a1})}{L_a(t_{a2})}, \quad \lambda_c = \frac{1}{t_{c2} - t_{c1}} \ln \frac{L_c(t_{c1})}{L_c(t_{c2})}. \tag{17}$$

Given that the values of λ_a and λ_c are found, the rate constants can be readily obtained by solving eqn (10) and (11) with respect to Bk_+ and k_- (see the **Supplementary Information**†). As a result, we have the following expressions for the sum $Bk_+ + k_- \equiv 1/t_{eq}$ and for each of the rates constants in terms of λ_a and λ_c:

$$\frac{1}{t_{eq}} = \frac{3(\lambda_a + \lambda_c) - t_{sep}\left(\lambda_a^2 + \lambda_c^2\right)}{3 - t_{sep}(\lambda_a + \lambda_c)} \tag{18}$$

$$Bk_+ = \left(1 + \frac{t_{sep}}{3t_{eq}}\right)\lambda_a - t_{sep}\,\lambda_a^2 \tag{19}$$

$$k_- = \left(1 + \frac{t_{sep}}{3t_{eq}}\right)\lambda_c - t_{sep}\,\lambda_c^2 \tag{20}$$

Here, expression (18) for $1/t_{eq}$ should be substituted in (19) and (20). Relations (17) use total amounts of the mixture of A* and C* in the peaks, whereas the experimental data, such as electropherograms, operate with signals (optical, electrochemical, *etc.*). Therefore, relations (17) have to be modified in such a way that the values of λ_a and λ_c are expressed in terms of signals from A* and C* rather than their total amounts. This can be easily done in a general case when signals are proportional to concentrations:

$$A_f^* = g_A A^*, \quad C_f^* = g_C C^* \tag{21}$$

were A_f^* and C_f^* are the signals generated by A* and C*, respectively. For example, in the case of fluorescence detection, the coefficients g_A and g_C can be expressed as follows:[39]

$$g_A = \frac{Q_A}{\chi_A}, \quad g_C = \frac{Q_C}{\chi_C} \tag{22}$$

Here, Q_A and Q_C are absolute quantum yields of A* and C* and χ_A and χ_C are proportionality coefficients.[41,42] They depend on fluorophores and detectors used for sensing A* and C*. Given relations (21), we have:

$$A_{fa}^* = g_A A_a^*, \quad C_{fa}^* = g_C C_a^*, \quad A_{fc}^* = g_A A_c^*, \quad C_{fc}^* = g_C C_c^* \tag{23}$$

Here, A_{fa}^* and C_{fa}^* are the total signals from A* and C* in zone A*. Similarly, A_{fc}^* and C_{fc}^* are the total signals from A* and C* in zone C*. Therefore,

$$\begin{aligned} L_{fa} &= A_{fa}^* + C_{fa}^* = g_A A_a^* + g_C C_a^*, \\ L_{fc} &= A_{fc}^* + C_{fc}^* = g_A A_c^* + g_C C_c^* \end{aligned} \tag{24}$$

were, L_{fa} and L_{fc} are the total signals from the mixture of A* and C* in zones A* and C*, respectively. Substitution of (8) and (9) into (24) leads to expressions for L_{fa} and L_{fc} that have the same structure as (15) and (16), *i.e.* L_{fa} and L_{fc} turn out to be proportional to $\exp(-\lambda_a t)$ and $\exp(-\lambda_c t)$, respectively. As a result, all considerations that lead to (17) remain valid for signals and, therefore, (17) holds if we replace the total amounts of the mixture of A* and C* (in zones A* and C*), L_a and L_c, with their total signals, L_{fa} and L_{fc}, respectively,

$$\lambda_a = \frac{1}{t_{a2} - t_{a1}} \ln \frac{L_{fa}(t_{a1})}{L_{fa}(t_{a2})}, \quad \lambda_c = \frac{1}{t_{c2} - t_{c1}} \ln \frac{L_{fc}(t_{c1})}{L_{fc}(t_{c2})} \tag{25}$$

Here, $L_{fa}(t_{a1})$ and $L_{fa}(t_{a2})$ are the total signals from the mixture of A* and C* in zone A* at times t_{a1} and t_{a2}, respectively. Similarly, $L_{fc}(t_{c1})$ and $L_{fc}(t_{c2})$ are the total signals from the mixture of A* and C* in zone C* at times t_{c1} and t_{c2}, respectively. Actually, one needs to know only the ratios of corresponding total signals that appear in (25) rather than the total signals themselves. These ratios can be estimated as ratios of the signal areas or even as ratios of the signal maxima corresponding to peaks A* and C* in spatial or temporal propagation patterns of the mixture of A* and C* (see the **Supplementary Information**†). Calculations based on peak heights are simpler than those based on peak areas since the former do not require the determination of boundaries of zones A* and C*.

Thus, to determine the rate constants, one should find the ratios of the total signals measured at two different times (in each of zones A* and C*). That can be achieved by placing a detector at different distances from the initial plug (Fig. 3). Practically this is achieved by performing 2 experiments with injections from different ends of the capillary. Then, parameters λ_a and λ_c should be determined from (25). Finally, the equilibration time t_{eq} and the rate constants k_+ and k_- are calculated using expressions (18)–(20). The concentration of B that appears in (19) should be known and chosen in such a way that heights of peaks A* and C* are of the same order of magnitude. The two-peak approximation can be applicable to the rate constant determination as soon as peaks A* and C* exist, which is always the case for slow and moderate-rate equilibration.

Test of applicability of the two-peak approximation to rate constant determination

To study the accuracy of finding k_+ and k_- using the two-peak approximation in KCE, we need to analyze temporal propagation patterns of components A* and C* participating in reaction (2) at various known values of k_+ and k_-. The best way to produce such patterns is to simulate them using the exact solution for eqn (4) at $B = const$.[38] A program, based on such exact solution, allows one to change basic parameters (k_+, k_-, v_A, v_C,

B, and W) and calculate simulated temporal propagation patterns of A* and C*. Then the latter can be utilized to back-calculate k_+ and k_- by using expressions (25) and (18)–(20). Since the true values of k_+ and k_- are known in this case, corresponding relative errors δ_+ and δ_- (an absolute value of the ratio between the deviation from the true value and the true value) are easy to determine. Of course, the exact solution for eqn (4) can also be used in the pattern-based approach to finding k_+ and k_-. However, the latter requires a fitting procedure that is computatively non-transparent and much more complicated than simple explicit expressions (18)–(20) and (25).

We simulated a total of 62 temporal propagation patterns of the mixture of A* and C* mimicking experimental electropherograms. They corresponded to various values of k_+, k_-, and B and to different positions of the detector. The values of the velocities and the initial plug width were $v_C = 0.09$ cm/s, $v_A = 0.06$ cm/s, and $W = 1.2$ cm, which are typical for capillary electrophoresis-based experiments. We assumed, for simplicity, that the signal is directly proportional to the total concentration of A* and B* ($g_A = g_C$). We also used the peak heights to estimate the ratio of the total signals (or the total amounts) of the mixture of A* and C* in zones A* and C*. A similar procedure based on peak areas rather than peak heights is discussed in the **Supplementary Information**.†

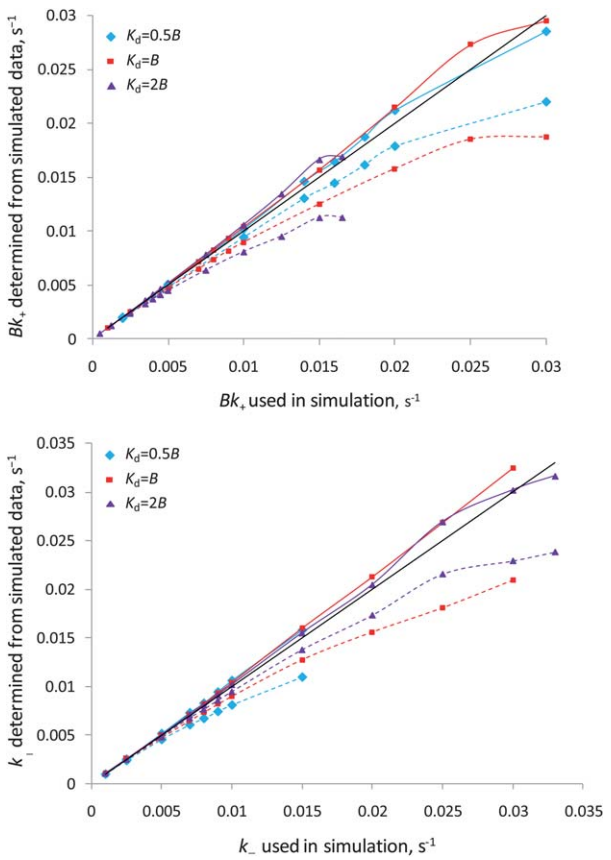

Fig. 4 Values of the rate constants determined from simulated "experiments" *versus* the rate constants used in simulations. The colored solid lines correspond to expressions (18)–(20), whereas the broken ones correspond to expression (14). The solid black lines show the ideal case (no errors). Three values of the K_d/B ratio (shown in the graphs) were used in calculations.

Results of these 62 "experimental" tests are presented in the two next figures. Fig. 4 shows dependencies of the rate constants determined by the two-peak approximation (the solid colored lines) on their values, used to produce simulated electropherograms. The broken colored lines depict values of the rate constants calculated using expressions (25) and, then, rough approximation (14), instead of more precise relations (18)–(20). The black solid lines in Fig. 4 correspond to the ideal case in which the determined rate constants would coincide with the ones used in simulation (the absence of any error). Fig. 5 shows dependencies of corresponding relative errors δ_+ and δ_- on the dimensionless parameter t_{sep}/t_{eq}. Again, the solid lines correspond to calculations based on expressions (25) in a combination with relations (18)–(20) whereas the broken lines correspond to calculations based on a combination of (25) and (14).

The upper limit of the rate constant ranges in Fig. 4 correspond to propagation patterns of the mixture of A* and C*, in which the peaks A* and C* shown in Fig. 3 would become almost undistinguishable. The same is true for the upper limit of the t_{sep}/t_{eq} ratio in Fig. 5. At higher values of this ratio, peaks A* and C* disappear entirely and the one-peak pattern immerges (Fig. 2c). The data in Fig. 5 shows that the two-peak approximation (based on relations (25) and (18)–(20)) facilitates the determination of the rate constants and insures relative errors lower than 10% in the entire range of conditions in which peaks A* and C* can be

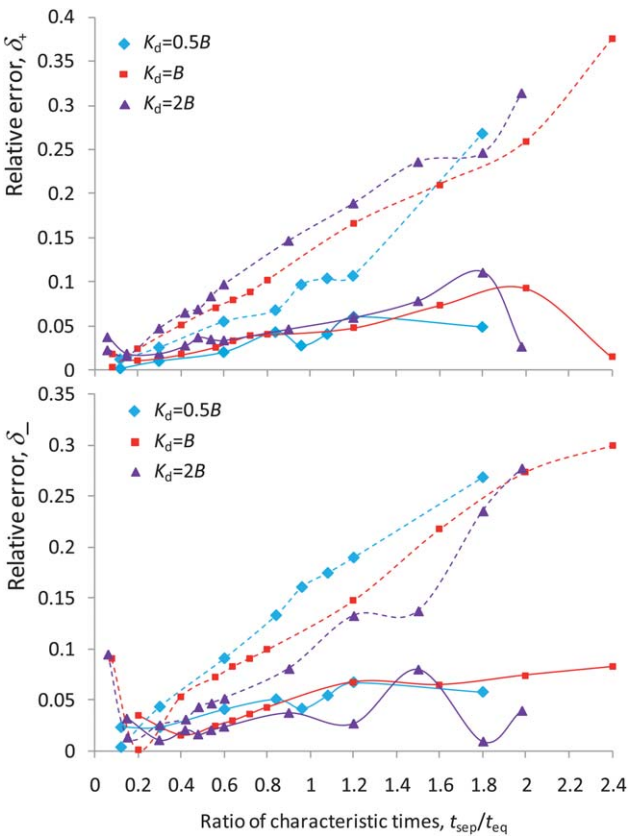

Fig. 5 Relative errors, δ_+ and δ_-, in the determination of k_+ and k_- *versus* the ratio of characteristic separation and equilibration times. Errors resulting from the use of (18)–(20) are shown by the solid lines whereas the ones resulted from the use of (14) are depicted by the broken lines.

identified. A comparison of the colored solid and broken lines in Fig. 5 shows that these errors are approximately 10 times smaller if the full solutions (18)–(20) are used instead of limiting expressions (14), derived at $t_{sep} \ll t_{eq}$. The improvement is significant even at small values of t_{sep}/t_{eq}.

Conclusions

In this work, we introduced a two-peak approximation in KCE that includes: (i) a new approximate analytical solution of mass-transfer equations for the non-equilibrium reaction (2) and (ii) a simple parameter-based method for finding rate constants k_+ and k_- for this reaction. We considered a general case with two requirements: (i) two peaks can be identified in electropherograms of reactants A* and C* (Fig. 2a and 2b) and (ii) $B = const$ in reaction (2). The constancy of B is readily achieved if B is present in access to A* and C* or if B is equilibrated with its dimer B_2 that is present in excess to B. In the latter case, B itself does not need to be in access to A* and C*. In such setups, the labeling of reactants A and C inside the plug serves only for their detection as no reactants A and C are present outside the plug. Finally, the constancy of B is "automatically" achieved in the MASKE setup. However, in this case, reactants A and C must be present outside the plug and equilibrated with A* and C* according to reaction (3). The two-peak approximation requires that two peaks corresponding to intact A* and C*, migrating with velocities of approximately v_A and v_C, be identifiable in propagation patterns of the mixture A* and C*. The presence of two identifiable peaks corresponds to the case of slow or moderate rate equilibration ($t_{sep} \ll t_{eq}$ or $t_{sep} \sim t_{eq}$). The parameters used in the method for finding k_+ and k_- are: (i) the total amounts of A* and C* (or the total signal from A* and C*) in the peaks and (ii) the travel times of the peaks to the detector. To exclude the need of knowing the initial amounts of A* and C* in the peaks, we suggest the use of reactors of two different lengths. The later will make the method applicable to practical separation techniques, such as capillary electrophoresis by using commercial instruments. We tested the accuracy of the two-peak approximation by applying it to 62 propagation patterns simulated with exact solution of eqn (4). We found that the method's accuracy was better than 10% for $t_{sep}/t_{eq} < 2.4$. Thus, the two-peak approximation provides a simple and effective way for studying rate constants of non-covalent interactions according to reaction (2). Given the fact that the two-peak approximation works for non-equilibrium reactions, it can be applied to various KCE methods. Finally, this approximation can be applied to the MASKE setup. Along with previously developed parameter-based method for fast equilibration,[38] the two-peak approximation creates a complete set of fitting-free approaches for finding k_+ and k_- in MASKE. This should also significantly increase MASKE effectiveness.

Acknowledgements

This work was funded by the Natural Sciences and Engineering Research Council of Canada.

References

1 S. Bell and A. Dutta, *Annu. Rev. Biochem.*, 2002, **71**, 333–374.
2 K. Kohn, *Mol. Biol. Cell*, 1999, **10**, 2703–2734.
3 I. Nooren and J. Thornton, *EMBO J.*, 2003, **22**, 3486–3492.
4 A. Ullrich and J. Schlessinger, *Cell*, 1990, **61**, 203–212.
5 P. von Hippel, D. G. Bear, W. D. Morgan and J. A. McSwiggen, *Annu. Rev. Biochem.*, 1984, **53**, 389–446.
6 M. Hashimoto, E. Rockenstein, L. Crews and E. Masliah, *NeuroMol. Med.*, 2003, **4**, 21–36.
7 S. B. Prusiner, *Proc. Natl. Acad. Sci. U. S. A.*, 1998, **95**, 13363–13383.
8 W. D. Wilson, *Science*, 2002, **295**, 2103–2105.
9 J. Østergaard, S. H. Hansen, H. Jensen and A. E. Thomsen, *Electrophoresis*, 2005, **26**, 4050–4054.
10 N. H. H. Heegaard, C. Schou and J. Østergaard, *Methods Mol. Biol.*, 2007, **421**, 303–338.
11 X. Liu, F. Dahdouh, M. Salgado and F. A. Gomez, *J. Pharm. Sci.*, 2009, **98**, 394–410.
12 Y. Sun, N. Fang and D. D. Y. Chen, *Electrophoresis*, 2008, **29**, 3333–3341.
13 S. N. Krylov, *J. Biomol. Screening*, 2006, **11**, 115–122.
14 V. Okhonin, S. M. Krylova and S. N. Krylov, *Anal. Chem.*, 2004, **76**, 1507–1512.
15 A. Petrov, V. Okhonin, M. Berezovski and S. N. Krylov, *J. Am. Chem. Soc.*, 2005, **127**, 17104–17110.
16 V. Okhonin, A. P. Petrov, M. Berezovski and S. N. Krylov, *Anal. Chem.*, 2006, **78**, 4803–4810.
17 G. G. Mironov, V. Okhonin, S. I. Gorelsky and M. V. Berezovski, *Anal. Chem.*, 2011, **83**, 2364–2370.
18 R. Bharadwaj, C. C. Park, I. Kazakova, H. Xu and J. S. Paschkewitz, *Anal. Chem.*, 2008, **80**, 129–134.
19 N. Fang and D. D. Y. Chen, *Anal. Chem.*, 2005, **77**, 840–847.
20 N. Fang and D. D. Y. Chen, *Anal. Chem.*, 2005, **77**, 2415–2420.
21 H. L. Wang and T. Li, *Anal. Chem.*, 2009, **81**, 1988–1995.
22 A. V. Petrov, L. T. Cherney, B. Dodgson, V. Okhonin and S. N. Krylov, *J. Am. Chem. Soc.*, 2011, **133**, 12486–12492.
23 P. Yang, Y. Mao, A. W.-M. Lee and R. T. Kennedy, *Electrophoresis*, 2009, **30**, 457–464.
24 A. L. Sloat, M. G. Roper, X. Lin, J. P. Ferrance, J. P. Landers and C. L. Colyer, *Electrophoresis*, 2008, **29**, 3446–3455.
25 E. J. Carrasco-Correa, M. Beneito-Cambra, J. M. Herrero-Martinez and G. Ramis-Ramos, *J. Chromatogr., A*, 2011, **1218**, 2334–2341.
26 Y. Z. Xu, X. J. Feng, W. Du, X. Liu, Q. M. Luo and B. F. Liu, *Anal. Chem.*, 2008, **80**, 6935–6941.
27 J. Zavaleta, D. Chinchilla, K. Martinez and F. A. Gomez, *J. Chromatogr., A*, 2006, **1105**, 59–65.
28 G. Hanrahan, R. E. Montes, A. Pao, A. Johnson and F. A. Gomez, *Electrophoresis*, 2007, **28**, 2853–2860.
29 J. Østergaard and H. Jensen, *Anal. Chem.*, 2009, **81**, 8644–8648.
30 S. D. Mendonsa and M. T. Bowser, *J. Am. Chem. Soc.*, 2004, **126**, 20–21.
31 S. F. Y. Li, J. Tok, J. Lai and T. Leung, *Electrophoresis*, 2010, **31**, 2055–2062.
32 M. Kanoatov, S. Javaherian and S. N. Krylov, *Anal. Chim. Acta*, 2010, **681**, 92–97.
33 D. T. Tran, K. P. F. Janssen, J. Pollet, E. Lammertyn, J. Anné, A. Van Schepdael and J. Lammertyn, *Molecules*, 2010, **15**, 1127–1140.
34 D. J. Turner, R. Tuytten, K. P. F. Janssen, J. Lammertyn, J. Wuyts, J. Pollet, S. Eyckerman, C. Brown and K. Kas, *Anal. Chem.*, 2011, **83**, 666–670.
35 B. Hornblower, A. Coombs, R. D. Whitaker, A. Kolomeisky, S. J. Picone, A. Meller and M. Akeson, *Nat. Methods*, 2007, **4**, 315–317.
36 W. Al-Soufi, B. Reija, M. Novo, S. Felekyan, R. Kuhnemuth and C. A. M. Seidel, *J. Am. Chem. Soc.*, 2005, **127**, 8775–8784.
37 Y. Li, G. J. Augustine and K. Weninger, *Biophys. J.*, 2007, **93**, 2178–2187.
38 V. Okhonin, M. V. Berezovski and S. N. Krylov, *J. Am. Chem. Soc.*, 2010, **132**, 7062–7068.
39 L. T. Cherney and S. N. Krylov, *Anal. Chem.*, 2011, **83**, 1381–1387.
40 L. T. Cherney, M. Kanoatov and S. N. Krylov, *Anal. Chem.*, 2011, **83**, 8617–8622.
41 A. Chartier, J. Georges and J. Mermet, *Chem. Phys. Lett.*, 1990, **171**, 347–352.
42 C. Parker and W. Rees, *Analyst*, 1960, **85**, 587–600.

SUPPLEMENTARY INFORMATION

Two-peak approximation in kinetic capillary electrophoresis

Leonid T. Cherney and Sergey N. Krylov

Department of Chemistry and Centre for Research on Biomolecular Interactions, York University, Toronto, Ontario, M3J 1P3, Canada

1. Derivation of ordinary differential equations for mass transfer in zones A* and C*

Mass transfer of A* and C* is described by the following equations:

$$\begin{aligned}(\partial_t + v_{\mathrm{A}}\partial_x)A^* &= -k_+ A^* B + k_- C^* \\ (\partial_t + v_{\mathrm{C}}\partial_x)C^* &= k_+ A^* B - k_- C^*\end{aligned} \quad . \tag{S1}$$

where ∂_x and ∂_t are partial derivations by the spatial coordinate x and time t, respectively; A^* and C^* are linear concentrations of A* and C*, respectively (i.e. amounts of A* and C* per unit length of the reactor); $B = const$ is a volume concentration of B; and v_{A} and v_{C} are the velocities of A* and C*; k_+ and k_- are the rate constants of the forward and reversed processes in the following equilibrium:

$$\mathrm{A}^* + \mathrm{B} \underset{k_-}{\overset{k_+}{\rightleftharpoons}} \mathrm{C}^* \tag{S2}$$

Let us consider propagation patterns in a case of slow ($t_{\mathrm{eq}} >> t_{\mathrm{sep}}$) or moderate-rate ($t_{\mathrm{eq}} \sim t_{\mathrm{sep}}$) equilibration. In this case, the two peaks, A* and C*, can be identified at the flanks of the label distribution (or the distribution of mixture of A* and C*). They move with velocities v_{A} and v_{C}, respectively (**Fig. S1**). As a result, the following transformations hold in zone A*:

$$\begin{aligned}&\frac{d}{dt}\int_{x_a^-}^{x_a^+} A^* dx = \int_{x_a^-}^{x_a^+} \frac{\partial A^*}{\partial t} dx + A^*\left(x_a^+\right)\frac{dx_a^+}{dt} - A^*\left(x_a^-\right)\frac{dx_a^-}{dt} = \\ &-\int_{x_a^-}^{x_a^+}\left(v_{\mathrm{A}}\frac{\partial A^*}{\partial x} + k_+ BA^* - k_- C^*\right)dx + v_{\mathrm{A}}\left[A^*\left(x_a^+\right) - A^*\left(x_a^-\right)\right] = \\ &-k_+ B\int_{x_a^-}^{x_a^+} A^* dx + k_-\int_{x_a^-}^{x_a^+} C^* dx\end{aligned} \tag{S3}$$

and

$$\frac{d}{dt}\int_{x_a^-}^{x_a^+} C^*\,dx = \int_{x_a^-}^{x_a^+} \frac{\partial C^*}{\partial t}\,dx + C^*\left(x_a^+\right)\frac{dx_a^+}{dt} - C^*\left(x_a^-\right)\frac{dx_a^-}{dt} =$$

$$-\int_{x_a^-}^{x_a^+}\left(v_{\mathrm{C}}\frac{\partial C^*}{\partial x} - k_+ BA^* + k_- C^*\right)dx + v_{\mathrm{A}}\left[C^*\left(x_a^+\right) - C^*\left(x_a^-\right)\right] = \qquad \text{(S4)}$$

$$k_+ B\int_{x_a^-}^{x_a^+} A^*\,dx - k_-\int_{x_a^-}^{x_a^+} C^*\,dx - \left(v_{\mathrm{C}} - v_{\mathrm{A}}\right)C^*\left(x_a^+\right)$$

.

Here, $x_a^-(t)$ and $x_a^+(t)$ are coordinates of the boundaries of zone A* (**Fig. S1**). To derive transformations (S3) and (S4), we used equations (S1) and the four following relations:

$$\int_{x_a^-}^{x_a^+}\frac{\partial A^*}{\partial x}dx = A^*\left(x_a^+\right) - A^*\left(x_a^-\right),\quad \int_{x_a^-}^{x_a^+}\frac{\partial C^*}{\partial x}dx = C^*\left(x_a^+\right) - C^*\left(x_a^-\right),\quad \frac{dx_a^\pm}{dt} = v_{\mathrm{A}},\quad C^*\left(x_a^-\right) = 0 \qquad \text{(S5)}$$

The last equation in (S5) follows from the fact that the concentration *C** vanishes at the left boundary of zone A*.

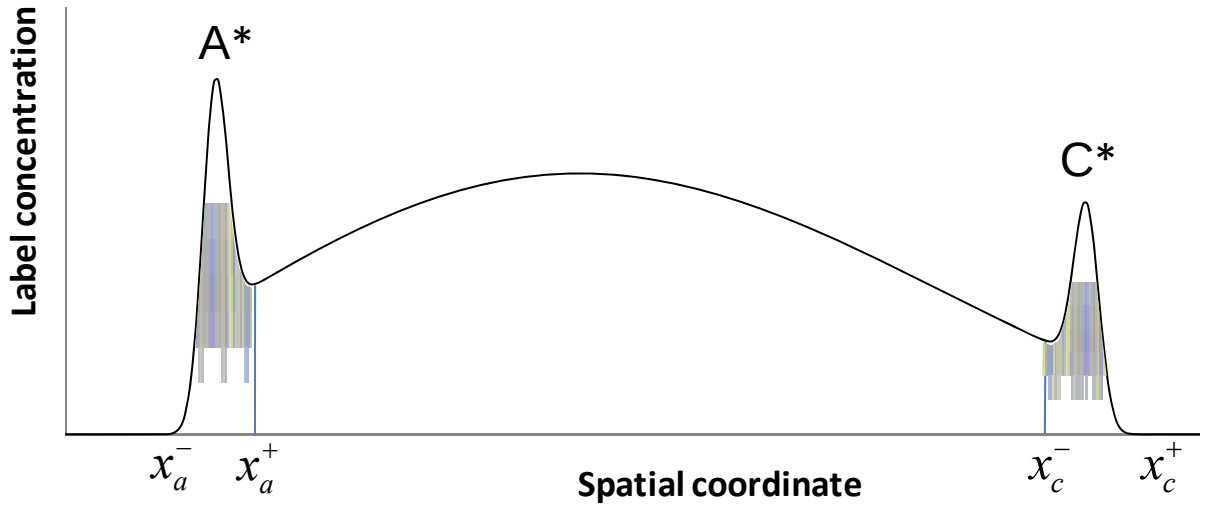

Figure S1. Spatial propagation pattern of the mixture of A* and C*. Their sum concentration coincides with that of the label. Areas corresponding to zones A* and C* are shaded. At $v_{\mathrm{C}} > v_{\mathrm{A}}$, zone C* is located to the right of zone A* (both zones move from left to right). Coordinates of the boundaries of zone A* are denoted by x^-_{a} and x^+_{a}, whereas coordinates of the boundaries of zone C* are denoted by x^-_{c} and x^+_{c}. At $k_- > Bk_+$, peak C* is lower than peak A*.

Transformations similar to (S3) and (S4) hold in zone C*:

$$\frac{d}{dt}\int_{x_c^-}^{x_c^+} A^*\,dx = \int_{x_c^-}^{x_c^+} \frac{\partial A^*}{\partial t}\,dx + A^*\left(x_c^+\right)\frac{dx_c^+}{dt} - A^*\left(x_c^-\right)\frac{dx_c^-}{dt} =$$

$$-\int_{x_c^-}^{x_c^+}\left(v_{\mathrm{A}}\frac{\partial A^*}{\partial x} + k_+ BA^* - k_- C^*\right)dx + v_{\mathrm{C}}\left[A^*\left(x_c^+\right) - A^*\left(x_c^-\right)\right] = \qquad \text{(S6)}$$

$$-k_+ B\int_{x_c^-}^{x_c^+} A^*\,dx + k_-\int_{x_c^-}^{x_c^+} C^*\,dx - \left(v_{\mathrm{C}} - v_{\mathrm{A}}\right)A^*\left(x_c^-\right)$$

.

and

$$\frac{d}{dt}\int_{x_c^-}^{x_c^+} C^*\,dx = \int_{x_c^-}^{x_c^+} \frac{\partial C^*}{\partial t}\,dx + C^*\left(x_c^+\right)\frac{dx_c^+}{dt} - C^*\left(x_c^-\right)\frac{dx_c^-}{dt} =$$

$$-\int_{x_c^-}^{x_c^+}\left(v_{\mathrm{C}}\frac{\partial C^*}{\partial x} - k_+ BA^* + k_- C^*\right)dx + v_{\mathrm{C}}\left[C^*\left(x_c^+\right) - C^*\left(x_c^-\right)\right] = \qquad \text{(S7)}$$

$$k_+ B\int_{x_c^-}^{x_c^+} A^*\,dx - k_-\int_{x_c^-}^{x_c^+} C^*\,dx$$

.

Here, $x_c^-(t)$ and $x_c^+(t)$ are coordinates of the left and right boundaries of zone C* (**Fig. S1**). To derive transformations (S4) and (S7), we again used equations (S1) and the following relations:

$$\int_{x_{\mathrm{C}}^-}^{x_{\mathrm{C}}^+}\frac{\partial A^*}{\partial x}dx = A^*\left(x_c^+\right) - A^*\left(x_c^-\right),\quad \int_{x_c^-}^{x_c^+}\frac{\partial C^*}{\partial x}dx = C^*\left(x_c^+\right) - C^*\left(x_c^-\right),\quad \frac{dx_c^\pm}{dt} = v_{\mathrm{C}},\quad A^*\left(x_c^+\right) = 0 \qquad \text{(S8)}$$

The last equation in (S8) follows from the fact that the concentration *A** approaches zero at the right boundary of zone C*.

Propagation patterns simulated with the exact solution of equations (S1) demonstrate the following behavior after introducing the initial plug containing compounds A* and C*. During time ~ t_{sep}, the peak corresponding to compound C* moves out of zone A* and the peak corresponding to compound A* moves out of zone C*. As a result, the distribution of C* in zone A* and the distribution of A* in zone C* become monotonic and can be approximated using power series:

$$C^*(x) = c_0 + c_1(x - x_a^-) + c_2(x - x_a^-)^2 + \ldots \qquad (x_a^- \le x \le x_a^+) \qquad \text{(S9)}$$

$$A^*(x) = a_0 + a_1(x - x_c^+) + a_2(x - x_c^+)^2 + \ldots \qquad (x_c^- \le x \le x_c^+) \qquad \text{(S10)}$$

Since $C^*(x)$ and $A^*(x)$ are smooth functions that vanish at x_{A}^- and x_{C}^+, respectively, we have:

$$c_0 = 0,\quad c_1 = 0,\quad a_0 = 0,\quad a_1 = 0\,. \qquad \text{(S11)}$$

Therefore:

$$\int_{x_a^-}^{x_a^+} C^* dx = \frac{c_2}{3}(x_a^+ - x_a^-)^3 + ..., \quad \int_{x_c^-}^{x_c^+} A^* dx = \frac{a_2}{3}(x_c^+ - x_c^-)^3 + ... \tag{S12}$$

By comparing expansions (S9) and (S10) to (S12) and taking into account only the leading terms in them, we obtain the following approximate relations:

$$C^*(x_a^+) \approx \frac{3}{x_a^+ - x_a^-}\int_{x_a^-}^{x_a^+} C^* dx, \quad A^*(x_c^-) \approx \frac{3}{x_c^+ - x_c^-}\int_{x_c^-}^{x_c^+} A^* dx \tag{S13}$$

Given expressions (S13), relations (S3), (S4), (S6), and (S7) can be rewritten in the form:

$$\frac{dA_a^*}{dt} = -k_+ B A_a^* + k_- C_a^*, \qquad \frac{dC_a^*}{dt} = k_+ B A_a^* - \left(k_- + \frac{3(v_C - v_A)}{W_a}\right) C_a^* \tag{S14}$$

$$\frac{dA_c^*}{dt} = -\left(k_+ B + \frac{3(v_C - v_A)}{W_c}\right) A_c^* + k_- C_c^*, \qquad \frac{dC_c^*}{dt} = k_+ B A_c^* - k_- C_c^* \tag{S15}$$

Here, A_a^* and C_a^* are the total amounts of A* and C* in the zone of A*:

$$A_a^* = \int_{x_a^-}^{x_a^+} A^* dx, \qquad C_a^* = \int_{x_a^-}^{x_a^+} C^* dx; \tag{S16}$$

A_c^* and C_c^* are the total amounts of A* and C* in the zone of C*:

$$A_c^* = \int_{x_c^-}^{x_c^+} A^* dx, \qquad C_c^* = \int_{x_c^-}^{x_c^+} C^* dx; \tag{S17}$$

W_a and W_c are the widths of zones A* and C* that are defined by expressions:

$$W_a = x_a^+ - x_a^-, \qquad W_c = x_c^+ - x_c^-. \tag{S18}$$

By taking into account the following definitions for t_{sep} and t_{eq}:

$$t_{sep} = \frac{W}{|v_C - v_A|}, \quad t_{eq} = \frac{1}{Bk_+ + k_-}, \tag{S19}$$

and by defining x_a^+ and x_c^- so that the widths of zones A* and C* , W_a and W_c, respectively, would coincide with the initial plug width W:

$$W_a = W, \quad W_c = W, \tag{S20}$$

we finally obtain ordinary differential equations for mass transfer:

$$\frac{dA_a^*}{dt} = -k_+ BA_a^* + k_- C_a^*, \quad \frac{dC_a^*}{dt} = k_+ BA_a^* - \left(k_- + \frac{3}{t_{\text{sep}}} \right) C_a^* \tag{S21}$$

$$\frac{dA_c^*}{dt} = -\left(k_+ B + \frac{3}{t_{\text{sep}}} \right) A_c^* + k_- C_c^*, \quad \frac{dC_c^*}{dt} = k_+ BA_c^* - k_- C_c^* \tag{S22}$$

Equations (S21) and (S22) are identical to equations (6) and (7) in the main text. They allow a significant simplification of the mathematical part of the developed parameter-based method for finding k_+ and k_-. At the same time, this simplification results in only 10% relative errors in the rate constants as was shown by our detailed study (the results are shown in **Fig. 5** of the main text). This accuracy is acceptable for most kinetic studies of biomolecular interactions.

2. Solutions to ordinary differential equations for mass transfer in zones A* and C*

System of linear differential equations (S21) has a critical point located at the origin in the phase plane (A^*_a, C^*_a) (**Fig. S2**). Similarly, system of equations (S22) has a critical point located at the origin in the plane (A^*_c, C^*_c).

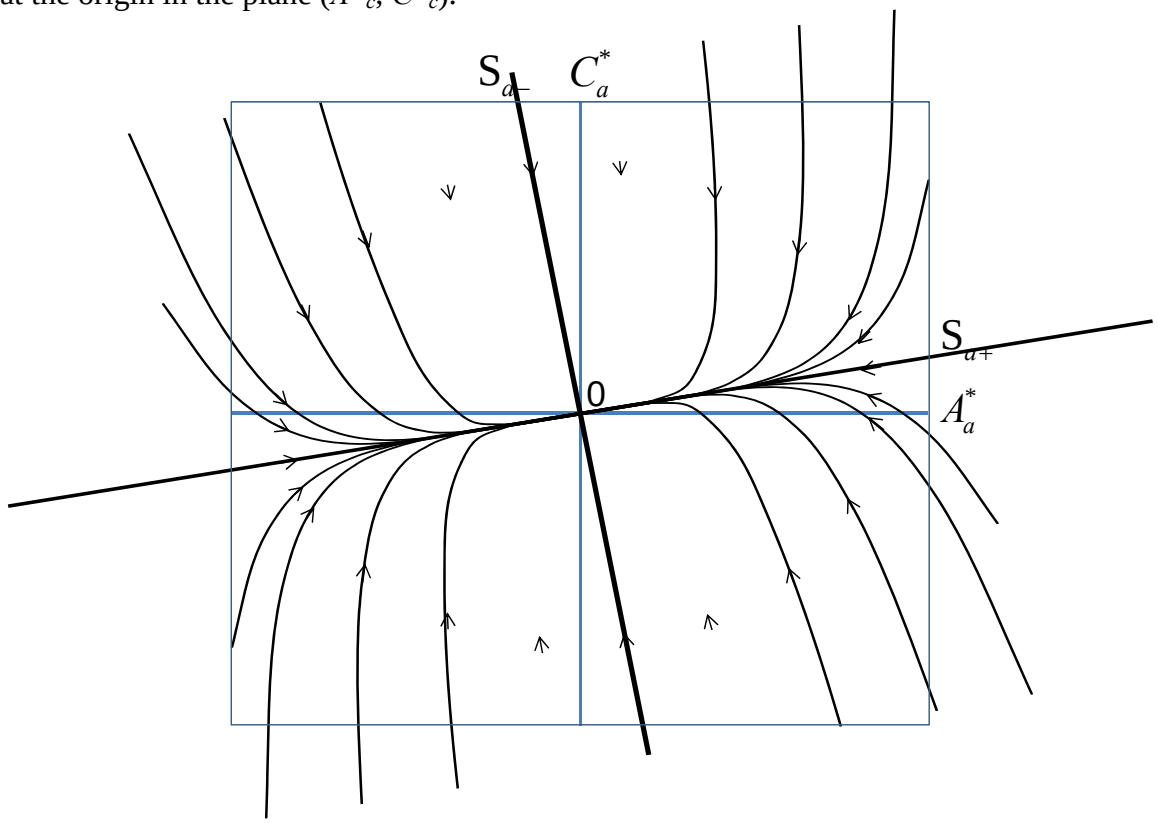

Figure S2. Qualitative phase portrait of system (S21). Its solutions are depicted by black lines in the plane (A_a^*, C_a^*). Arrows show directions in which time increases. The thick straight lines represent solutions that satisfy the first condition from (S27). Rays OS_{a+} and OS_{a-} intersect at a right angle if $K_\text{d} = B$. The ray OS_{a+} corresponds to the special solution (S34) and, therefore, $\tan \angle A_a^* 0 S_{a+} = \eta_a$. The phase portrait of system (S22) looks similar.

Let us denote eigenvalues of (S21) as $-\lambda_{a\pm}$ and eigenvalues of (S21) as $-\lambda_{c\pm}$. These eigenvalues satisfy quadratic equations that follow from (S21) and (S22):

$$\lambda_{a\pm}^2 - \left(Bk_+ + k_- + \frac{3}{t_{\text{sep}}} \right) \lambda_{a\pm} + \frac{3Bk_+}{t_{\text{sep}}} = 0 \tag{S23}$$

$$\lambda_{c\pm}^2 - \left(Bk_+ + k_- + \frac{3}{t_{\text{sep}}} \right) \lambda_{c\pm} + \frac{3k_-}{t_{\text{sep}}} = 0 \tag{S24}$$

Roots of (S23) and (S24) are determined by expressions:

$$\lambda_{a\pm} = \frac{1}{2}\left(Bk_+ + k_- + \frac{3}{t_{\text{sep}}} \right) \pm \sqrt{\frac{1}{4}\left(Bk_+ + k_- + \frac{3}{t_{\text{sep}}} \right)^2 - \frac{3Bk_+}{t_{\text{sep}}}} \tag{S25}$$

$$\lambda_{c\pm} = \frac{1}{2}\left(Bk_+ + k_- + \frac{3}{t_{\text{sep}}} \right) \pm \sqrt{\frac{1}{4}\left(Bk_+ + k_- + \frac{3}{t_{\text{sep}}} \right)^2 - \frac{3k_-}{t_{\text{sep}}}} \tag{S26}$$

Here, plus and minus signs in subscripts (at $\lambda_{a\pm}$ and $\lambda_{c\pm}$) correspond, respectively, to plus and minus signs in front of the radicals. Obviously, both eigenvalues $-\lambda_{a\pm}$ are real, distinct and negative. The same is true for eigenvalues $-\lambda_{c\pm}$. Therefore, both critical points are improper stable nodes.[1,2] All solutions to system (S21) approach the point $A_a^* = 0,\ C_a^* = 0$ and all solutions to system (S22) approach the point $A_c^* = 0,\ C_c^* = 0$ (**Fig. S2**). In physical terms, such a behavior means that peaks A* and C* gradually decrease and eventually disappear with increasing time. As a result of this relaxation process, all compounds A* and C* will be distributed over the "bridge". It is well known that solutions to a system of two ordinary differential equations can approach an improper stable node with distinct eigenvalues only in two directions.[1,2] Therefore, we have at $t \to \infty$:

$$\frac{C_a^*(t)}{A_a^*(t)} = \eta_{a\pm} = const, \qquad \frac{A_c^*(t)}{C_c^*(t)} = \eta_{c\pm} = const\ . \tag{S27}$$

where the plus and minus signs in subscripts correspond to these different directions. Only non-negative values of $\eta_{a\pm}$ and $\eta_{c\pm}$ can describe physical processes since concentrations of A* and C* are non-negative quantities. This non-negativity condition for $\eta_{a\pm}$ and $\eta_{c\pm}$ fixes one possible direction in each node. Systems (S21) and (S22) have special solutions that satisfy (S27) at all $t \geq 0$ rather than at $t \to \infty$. They correspond to straight lines in the phase planes (A_a^*, C_a^*) and (A_c^*, C_c^*) (**Fig. S2**). To find such solutions, we have to substitute $C_a^*(t) = \eta_{a\pm} A_a^*(t)$ into system

(S21) and to substitute $A_c^*(t) = \eta_{c\pm} C_c^*(t)$ into system (S22). As a result, the following quadratic equations for $\eta_{a\pm}$ and $\eta_{c\pm}$ can be obtained:

$$k_- \eta_{a\pm}^2 - \left(Bk_+ - k_- - \frac{3}{t_{\text{sep}}} \right) \eta_{a\pm} - Bk_+ = 0 \tag{S28}$$

and

$$Bk_+ \eta_{c\pm}^2 - \left(k_- - Bk_+ - \frac{3}{t_{\text{sep}}} \right) \eta_{c\pm} - k_- = 0 \tag{S29}$$

Roots of these equations are determined by expressions

$$\eta_{a\pm} = \frac{1}{k_-} \left\{ \frac{1}{2} \left(Bk_+ - k_- - \frac{3}{t_{\text{sep}}} \right) \pm \sqrt{\frac{1}{4} \left(Bk_+ - k_- - \frac{3}{t_{\text{sep}}} \right)^2 + Bk_+ k_-} \right\} \tag{S30}$$

and

$$\eta_{c\pm} = \frac{1}{Bk_+} \left\{ \frac{1}{2} \left(k_- - Bk_+ - \frac{3}{t_{\text{sep}}} \right) \pm \sqrt{\frac{1}{4} \left(k_- - Bk_+ - \frac{3}{t_{\text{sep}}} \right)^2 + Bk_+ k_-} \right\} \tag{S31}$$

The plus signs in front of the radicals obviously correspond to positive roots $\eta_a \equiv \eta_{a+}$ and $\eta_c \equiv \eta_{c+}$. Expressions (S30) and (S31) for these roots can be rewritten as follows:

$$\eta_a = \frac{Bk_+ - \lambda_a}{k_-} \geq 0, \qquad \eta_c = \frac{k_- - \lambda_c}{Bk_+} \geq 0, \tag{S32}$$

where $\lambda_a \equiv \lambda_{a-}$ and $\lambda_c \equiv \lambda_{c-}$. Given expression (S25) and (S26) for λ_{a-} and λ_{c-}, we also have:

$$\lambda_a = \Omega - \sqrt{\Omega^2 - \frac{3Bk_+}{t_{\text{sep}}}}, \quad \lambda_c = \Omega - \sqrt{\Omega^2 - \frac{3k_-}{t_{\text{sep}}}}, \quad \Omega \equiv \frac{1}{2} \left(Bk_+ + k_- + \frac{3}{t_{\text{sep}}} \right). \tag{S33}$$

Finally, direct substitutions of expressions:

$$A_a^* = N_a \exp(-\lambda_a t), \quad C_a^* = \eta_a N_a \exp(-\lambda_a t), \tag{S34}$$

and

$$A_c^* = \eta_c N_c \exp(-\lambda_c t), \quad C_c^* = N_c \exp(-\lambda_c t) \tag{S35}$$

into equations (S21) and (S22), respectively, show that (S34) and (S35) are solutions to these equations. Here, N_a and N_c are constant coefficients that relate to initial amounts A_0^* and C_0^* of compounds A* and C* in the plug:

$$N_a + \eta_c N_c = A_0^*, \qquad \eta_a N_a + N_c = C_0^*. \tag{S36}$$

Obviously, solutions (S34) and (S35) also satisfy conditions (S27) with positive values of constants. These solutions are represented by the ray OS_{a+} in **Fig. S2** and by a similar ray (that should be denoted as OS_{c+}) in the phase portrait of system (S22).

If $t_{sep} << t_{eq}$, we have from definitions (S33) for Ω and (S19) for t_{sep} and t_{eq}:

$$\frac{3Bk_+}{t_{sep}\Omega^2} = \frac{12Bk_+}{t_{sep}\left(Bk_+ + k_- + \frac{3}{t_{sep}}\right)^2} < \frac{12t_{sep}}{t_{eq}\left(\frac{t_{sep}}{t_{eq}} + 3\right)^2} < \frac{4t_{sep}}{3t_{eq}} \ll 1 \qquad \text{(S37)}$$

$$\frac{3k_-}{t_{sep}\Omega^2} = \frac{12Bk_-}{t_{sep}\left(Bk_+ + k_- + \frac{3}{t_{sep}}\right)^2} < \frac{12t_{sep}}{t_{eq}\left(\frac{t_{sep}}{t_{eq}} + 3\right)^2} < \frac{4t_{sep}}{3t_{eq}} \ll 1 \qquad \text{(S38)}$$

In this case, expressions (S33) can be expanded in small parameter t_{sep}/t_{eq}. As a result, we obtain the following asymptotic relations (to the first order in t_{sep}/t_{eq}):

$$\lambda_a = \Omega - \Omega\sqrt{1 - \frac{3Bk_+}{t_{sep}\Omega^2}} \simeq \Omega - \Omega\left(1 - \frac{3Bk_+}{2t_{sep}\Omega^2}\right) = \frac{3Bk_+}{2t_{sep}\Omega} = Bk_+\left(1 + \frac{t_{sep}}{3t_{eq}}\right)^{-1} \simeq Bk_+\left(1 - \frac{t_{sep}}{3t_{eq}}\right) \qquad \text{(S39)}$$

$$\lambda_c = \Omega - \Omega\sqrt{1 - \frac{3k_-}{t_{sep}\Omega^2}} \simeq \Omega - \Omega\left(1 - \frac{3k_-}{2t_{sep}\Omega^2}\right) = \frac{3k_-}{2t_{sep}\Omega} = k_-\left(1 + \frac{t_{sep}}{3t_{eq}}\right)^{-1} \simeq k_-\left(1 - \frac{t_{sep}}{3t_{eq}}\right). \qquad \text{(S40)}$$

Therefore, λ_a and λ_c approach Bk_+ and k_-, respectively, if the ratio t_{sep}/t_{eq} approaches zero. At small values of t_{sep}/t_{eq} we obtain:

$$\lambda_a \approx Bk_+, \quad \lambda_c \approx k_- \qquad (t_{sep}/t_{eq} \ll 1), \qquad \text{(S41)}$$

Relations (S32) – (S35) and (S41) are identical to relations (8) – (14) in the main text.

Given (S25) and (S26), the following inequalities are fulfilled for the absolute values of eigenvalues:

$$\frac{\lambda_{a+}}{\lambda_{a-}} > 1, \qquad \frac{\lambda_{c+}}{\lambda_{c-}} > 1. \qquad \text{(S42)}$$

Therefore, using a general theory of dynamic systems,[1,2] we can conclude that all (but two) solutions to system (S21) approach the critical point of (S21) in the same direction as the special solution (S34) (**Fig. S2**). Similarly, all (but two) solutions to system (S22) approach the critical point of (S22) in the same direction as the special solution (S35). Thus, solutions (S34) and (S35) are stable. Actually, the ratios (S37) are significantly larger than unity (for example, they are more than 5.83 at $K_d = B$). Because of this fact, the convergence of other solutions to the special solutions (S34) and (S35) occurs relatively quickly (**Fig. S2**). As a result, special solutions can be considered good candidates to describe processes of relaxation of peaks A* and C*. One could expect that they describe the relaxation that occurs at the maximum speed and, therefore, takes place in reality.

3. Determination of the rate constants k_+ and k_- based on the total amounts of the mixture of A* and C* in zones A* and C*

Taking into account (S34) and (S35), we have:

$$L_a(t_{a1}) \equiv A_a^* + C_a^* = (1+\eta_a) N_a \exp(-\lambda_a t_{a1}), \quad L_c(t_{c1}) \equiv A_c^* + C_c^* = (1+\eta_c) N_c \exp(-\lambda_c t_{c1}), \tag{S43}$$

$$L_a(t_{a2}) \equiv A_a^* + C_a^* = (1+\eta_a) N_a \exp(-\lambda_a t_{a2}), \quad L_c(t_{c2}) \equiv A_c^* + C_c^* = (1+\eta_c) N_c \exp(-\lambda_c t_{c2}). \tag{S44}$$

Here L_a and L_c are the total amounts of the label (or the mixture of A* and C*) in zones A* and C*, respectively; t_{a1} and t_{a2} are two different times at which L_a is measured; similarly, t_{c1} and t_{c2} are two (other) different times at which L_c is measured. It is obvious from relations (S43) and (S44) that:

$$\frac{L_a(t_{a1})}{L_a(t_{a2})} = \exp\left[\lambda_a (t_{a2} - t_{a1})\right], \quad \frac{L_c(t_{c1})}{L_c(t_{c2})} = \exp\left[\lambda_c (t_{c2} - t_{c1})\right]. \tag{S45}$$

By solving (S45) with respect to λ_a and λ_c, we obtain the following expressions for them in terms of the measurable quantities (L_a, L_c, t_{a1}, t_{a2}, t_{c1}, t_{c2}):

$$\lambda_a = \frac{1}{t_{a2} - t_{a1}} \ln \frac{L_a(t_{a1})}{L_a(t_{a2})}, \quad \lambda_c = \frac{1}{t_{c2} - t_{c1}} \ln \frac{L_c(t_{c1})}{L_c(t_{c2})}. \tag{S46}$$

They coincide with relations (17) from the main text. On the other hand, λ_a and λ_c can be expressed in terms of rate constants, k_+ and k_-, using (S33). Remarkably, to determine k_+ and k_-, we actually do not need to solve algebraic equations (S33) containing radicals. The rate constants can be easily expressed in terms of λ_a and λ_c, using relations (S23) and (S24). The latter form a system of liner algebraic equations with respect to k_+ and k_-. By adding up (S23) and (S24), we obtain an equation that can be readily solved with respect to $Bk_+ + k_- \equiv 1/t_{\text{eq}}$. As a result,

$$\frac{1}{t_{\text{eq}}} \equiv Bk_+ + k_- = \frac{3(\lambda_a + \lambda_c) - t_{\text{sep}}(\lambda_a^2 + \lambda_c^2)}{3 - t_{\text{sep}}(\lambda_a + \lambda_c)}. \tag{S47}$$

Then, by solving (S23) and (S24) with respect to Bk_+ and k_-, we finally obtain:

$$Bk_+ = \left(1 + \frac{t_{\text{sep}}}{3t_{\text{eq}}}\right)\lambda_a - t_{\text{sep}}\lambda_a^2, \quad k_- = \left(1 + \frac{t_{\text{sep}}}{3t_{\text{eq}}}\right)\lambda_c - t_{\text{sep}}\lambda_c^2. \tag{S48}$$

Here, $1/t_{\text{eq}}$ is presumed to be expressed in terms of λ_a and λ_c, using (S47). Solutions (S47) and (S48) coincide with relations (18) – (20) in the main text. It is obvious from (S46) – (S48) that the rate constants are completely determined by $L_a(t_{a1})/L_a(t_{a2})$ and $L_c(t_{c1})/L_c(t_{c2})$, i.e. by the ratios of the amounts of the label (or the mixture of A* and C*) measured at two different times in zones A* and C*. Total amounts L_a and L_c in (S46) can be replaced by total signals L_{fa} and

L_{fc} from zones A* and C*, respectively, as it is explained in the main text. Then ratios $L_{fa}(t_{a1})/L_{fa}(t_{a2})$ and $L_{fc}(t_{c1})/L_{fc}(t_{c2})$ can be calculated using the areas of corresponding zones in spatial or temporal propagation patterns of the label (or the mixture of A* and C*) (**Fig. S1**), given the following relations between these areas:

$$\int_{x_a^-}^{x_a^+} L_{fa}(x,t_{a1})dx = v_{\mathrm{A}} \int_{t_a^+}^{t_a^-} L_{fa}(x_1,t)dt, \quad \int_{x_c^-}^{x_c^+} L_{fc}(x,t_{c1})dx = v_{\mathrm{C}} \int_{t_c^+}^{t_c^-} L_{fc}(x_1,t)dt, \tag{S49}$$

$$\int_{x_a^-}^{x_a^+} L_{fa}(x,t_{a2})dx = v_{\mathrm{A}} \int_{t_a^+}^{t_a^-} L_{fa}(x_2,t)dt, \quad \int_{x_c^-}^{x_c^+} L_{fc}(x,t_{c2})dx = v_{\mathrm{C}} \int_{t_c^+}^{t_c^-} L_{fc}(x_2,t)dt \tag{S50}$$

Here, t_a^+ and t_a^- are moments of time in the temporal propagation pattern of zone A* corresponding to the boundaries x_a^+ and x_a^- in its spatial propagation pattern. Similarly, t_c^+ and t_c^- are moments of time in the temporal propagation pattern of zone C* corresponding to the boundaries x_c^+ and x_c^- in its spatial propagation pattern. Obviously, $t_a^+ < t_a^-$ and $t_c^+ < t_c^-$ since right boundaries x_a^+ and x_c^+ reach the detector earlier than corresponding left boundaries x_a^- and x_c^-. The above considerations are based on definitions of the right and left boundaries (x_a^+ and x_c^-) for zones A* and C*, respectively, that lead to relations (S20). These "inner" boundaries of zones A* and C* could be defined in some other way, for example, as coordinates of the local minimums in the concentration of the label (or the mixture of A* and C*) (**Fig. S1**). These minimums can be found at the flanks of the "bridge" connecting zones A* and C*. Let us assume that widths W_a and W_c of such redefined zones A* and C* remain approximately constant with time but differ significantly from W. Then, the above results will remain valid after the following modification. If $W_a \approx W_c$ one should just use W_a or W_c (instead of W) in definition (S19) for t_{sep}. In more general case, when W_a and W_c vary considerably, different separation times:

$$t_a = \frac{W_a}{|v_{\mathrm{C}} - v_{\mathrm{A}}|}, \quad t_c = \frac{W_c}{|v_{\mathrm{C}} - v_{\mathrm{A}}|} \tag{S51}$$

should be used in zones A* and C*, respectively. Thus, all above results related to zone A* will hold true if t_{sep} is replaced with t_a in the corresponding equations. Similarly, results related to zone C* will hold true if t_{sep} is replaced with t_c. However, expressions (S47) and (S48) for the rate constants cannot be modified in such a way. Indeed, to derive (S47) and (S48), we used the fact that both (S23) and (S24) contain the same parameter t_{sep}. It should be replaced with t_a (in equation (S23) or with t_c (in equation (S24)), if the widths W_a and W_c of zones A* and C* are different. After such a modification of equations (S23) and (S24), their solutions cannot be found by the simple way described. Instead, one should apply Cramer's rule.[3] As a result, expressions for Bk_+ and k_- become more cumbersome. Moreover, this procedure requires complex processing of experimental data to identify boundaries of zones A* and C*.

References

1 Hirsch, M. W.; Smale, S. ; Devaney, R. *Differential Equations, Dynamical Systems, and an Introduction to Chaos* (2nd ed.); Academic Press, 2003 (425 pages).

2 Jordan, D. W.; Smith, P. *Nonlinear Ordinary Differential Equations* (4th ed.); Oxford University Press, 2007 (540 pages).

3 Leon, S. J. *Linear Algebra with Applications* (7th ed.), Pearson Prentice Hall, 2006 (544 pages).